Particle dynamics at fluid interfaces studied by the color gradient lattice Boltzmann method coupled with the smoothed profile method

Young Ki Lee and Kyung Hyun Ahn*

School of Chemical and Biological Engineering, Institute of Chemical Processes, Seoul National University, Seoul, 08826, Korea

(Received 13 December 2019; revised manuscript received 30 March 2020; accepted 12 April 2020; published 7 May 2020)

We suggest a numerical method to describe particle dynamics at the fluid interface. We adopt a coupling strategy by combining the color gradient lattice Boltzmann method (CGLBM) and smoothed profile method (SPM). The proposed scheme correctly resolves the momentum transfer among the solid particles and fluid phases while effectively controlling the wetting condition. To validate the present algorithm (CGLBM-SPM), we perform several simulation tests like wetting a single solid particle and capillary interactions in two solid particles floating at the fluid interface. Simulation results show a good agreement with the analytical solutions available and look qualitatively reasonable. From these analyses, we conclude that the key features of the particle dynamics at the fluid interface are correctly resolved in our simulation method. In addition, we apply the present method for spinodal decomposition of a ternary mixture, which contains two-immiscible fluids with solid particles. By adding solid particles, fluid segregation is much suppressed than in the binary liquid mixture case. Furthermore, it has different morphology, such as with the jamming structure of the particles at the fluid interface, and captured images are similar to bicontinuous interfacially jammed emulsion gels in literature. From these results, we confirm the feasibility of the present method to describe soft matters; in particular, emulsion systems that contain solid particles at the interface.

DOI: 10.1103/PhysRevE.101.053302

I. INTRODUCTION

The last decade witnessed an increasing interest in colloidal particles at the fluid interface, which is due to a wide application of fluid-particle mixture systems. The self-assembly of colloidal particles at the fluid interface enabled the preparation of high-quality two-dimensional crystals [1,2]. In particular, Langmuir trough techniques provide a means to tune the interparticle distances and facilitate the transfer of the crystal monolayers to solid substrates [3]. Solid particles at the fluid interface play important roles in many processes involving foams and emulsions [4–7]. It has been known for many years that the solid particles at the interface can be exploited to tune the stability of emulsions, and now they are applied in pharmaceutical, food, oil, and cosmetic industries. Even though there are signs of progress for understanding these complex systems, little information is available on its dynamics in particular. The description of the forces determining the physical behavior of the solid particles at the fluid interface still remains a challenge in modern colloid science, and more intensive study is required.

Recently, numerical simulations have been applied to investigate the dynamics of solid particles at the fluid interface. The lattice Boltzmann method (LBM) has received considerable attention as a promising tool to probe such a complex system. Onishi *et al.* [8] suggested a numerical algorithm based on the Shan-Chen (SC) multiphase model where mesoscopic interactions are introduced among different fluid phases to incorporate interfacial tension [9]. They modified the original SC model to consider a solid phase and described the capillary interactions on the particle. Joshi and Sun [10] applied a slightly different variation of the SC model. They used the single component multiphase model (SCMP) and coupled it with the Ladd's model [11,12], which describes the solid particle in a solvent. They validated their algorithm through several tests and applied this to the colloidal droplet drying problem [13]. Jansen and Harting [14] followed a similar strategy with Joshi and Sun, but they applied the multicomponent multiphase model like Onishi *et al.* Solid particles were still described by Ladd's model, but the area around and inside solid particles were more strictly treated to enhance mass conservation and also to control the wettability of the particles. They also demonstrated the applicability of their algorithm for the phase transition of liquid-solid mixtures, such as bicontinuous interfacially jammed emulsion gels (bijels) and Pickering emulsions. This method was recently extended for a more complex system involving ellipsoid particles in multicomponent fluids [15].

As reviewed above, several studies were carried out using LBM to describe particle dynamics in the multiphase fluid system. Although the methods based on SC captured qualitatively and, in some points, quantitatively reasonable results for target systems, unsolved numerical problems remain. For example, Joshi and Sun [10] reported an artificial motion of a solid particle around a droplet interface. They showed the unphysical particle motion caused by high spurious velocities that are driven by poor numerical stability of the SC model. In

*Corresponding author: ahnnet@snu.ac.kr

addition, other inherent limitations of the original SC model have been found as well, such as poor numerical stability for unequal fluid densities or viscosities and incorrect mass conservation [16–19]. The numerical errors caused by these inherent defects in the SC model may become severe when they couple with other algorithms including solid particles, and eventually unphysical results will be obtained as in Ref [10]. Therefore, developing more robust numerical models for the multiphase fluids and a strategy to couple fluid and solid particles are highly required in the field.

In an effort to develop a multiphase model, various algorithms have been introduced in the LBM framework such as the free-energy based model suggested by Swift *et al.* [20] and a mean field theory based approach introduced by He *et al.* [21]. As an alternative approach, Gunstensen *et al.* [22] proposed the color gradient lattice Boltzmann method (CG or CGLBM), which is based on the lattice-gas model of Rothman and Keller [23].

Recently, there has been significant progress in CGLBM. Grunau *et al.* [24] introduced a modified form of distribution function to enable different density and viscosity ratios in CGLBM. Latva-Kokko and Rothman [25] replaced Gunstensen's maximization-recoloring step with a formulaic segregation algorithm to solve two numerical issues in the previous CGLBM; namely, the lattice-pinning effect and spurious velocities at the interface. Reis and Phillips [26] modified the perturbation operator to correctly recover the Navier-Stokes equations. Leclaire *et al.* [27] combined Latva-Kokko–Rothman's recoloring operator [25] with Reis-Phillips' perturbation operator [26] to improve the numerical stability and accuracy of the CGLBM. Also, they adopted an isotropic gradient operator to enhance the numerical stability and accuracy of the model [28]. Liu *et al.* [29] derived a generalized perturbation operator using the phase-field and formulated the CGLBM for a three-dimensional (3D) system. Leclaire *et al.* [18] generalized the CGLBM to two and three dimensions. Recently, Wen *et al.* [30] enhanced the 3D CGLBM and improved remaining issues in the model, such as the lack of Galilean invariance and error terms in the recovered macroscopic equations.

Thanks to the pioneers' investigations, CGLBM has now become one of the most robust numerical methods to describe the multiphase system. However, this model is only adaptable for liquid systems with no solid particles yet. Inspired by this limitation, we suggest a numerical method that can effectively describe particle dynamics in the fluid interface in the CGLBM framework. Our method is established on the CGLBM with the smoothed profile method (SPM) [31,32] to describe the particle dynamics in fluids. To validate our method (CGLBM-SPM), we carried out several benchmark tests in the study. The wettability of a single particle and capillary interactions between two-solid particles were carefully studied. In addition, spinodal decomposition of a ternary mixture, which includes solid particles and immiscible fluids, was tested as an example to show the potential of this algorithm. In all the simulation results, the new algorithm showed great performance and potential as a simulation tool. To the best of our knowledge, there is no previous report that couples solid particles with multiphase fluids described by CGLBM. We believe that our numerical method is quite robust and useful in studying classical fluid dynamics and soft matter physics.

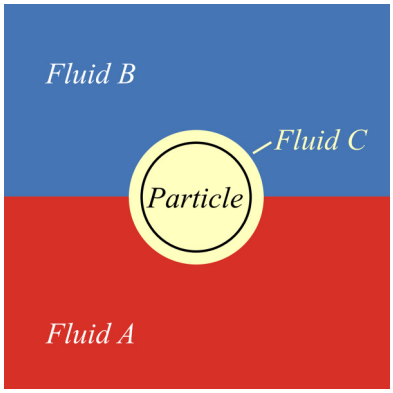

FIG. 1. The schematic diagram of the system.

This paper is organized as follows: The details of the simulation method are presented in Sec. II. The simulation setup and results that validate the algorithm are provided in Sec. III. The wetting boundary effect of a single particle at the fluid interface is described in Sec. III A and the capillary interactions between two solid particles are carefully analyzed in Sec. III B. The application to spinodal decomposition of ternary mixtures is described in Sec. III C. Finally, conclusions are drawn in Sec. IV.

II. NUMERICAL METHODS

In the present study, the LBM is applied as a solver to describe the complex systems in which rigid particles are immersed at the fluid interface. Multiphase fluids are described by the CGLBM and it is combined with the SPM, which describes the motion of solid particles. In the algorithm, immiscible fluids A and B are considered, and also fluid C is additionally introduced for the purpose of controlling the wettability of the solid particle. The particle is always entrapped in fluid C, which remains fully wetted condition as described in Fig. 1. The solid particle transfers the momentum with all the fluids around, and finally, hydrodynamic interactions are correctly resolved. In this section, we describe the details of each algorithm and the strategy utilized to couple them.

A. Color gradient lattice Boltzmann method (CGLBM)

Since the CGLBM was introduced by Gunstensen *et al.* [22], it has been improved by pioneers to become one of the most robust tools to investigate multiphase flows. Due to its accuracy and flexibility, CGLBM has been applied to various multiphase problems like flow in porous media [18,33], droplet formation in microfluidic devices [34,35], and droplet dynamics with insoluble surfactants [36,37].

In this study, we follow the CGLBM presented by Leclaire *et al.* [38], which describes a three component system. Three sets of distribution functions are required to track the evolution of fluid components, which occur via a streaming and collision process. These processes are given by the equation

below:

$$f_i^k(\mathbf{x}+\mathbf{c}_i\Delta t, t+\Delta t) = f_i^k(\mathbf{x},t) + \Omega_i^k\left(f_i^k(\mathbf{x},t)\right) + F_i\Delta t. \tag{1}$$

Here, the distribution function for fluid k (e.g., $k = A$, B, and C) is denoted as f^k and F is an external body force imposed on the fluid.

In this study, the D2Q9 lattice model was employed as it considers nine directional velocities in a 2D space. For D2Q9, the lattice velocity vectors are given by

$$[\mathbf{c}_0, \mathbf{c}_1, \cdots \mathbf{c}_8] = \begin{bmatrix} 0 & 1 & 0 & -1 & 0 & 1 & -1 & -1 & 1 \\ 0 & 0 & 1 & 0 & -1 & 1 & 1 & -1 & -1 \end{bmatrix}. \tag{2}$$

Here, Ω_i^k denotes the combination of three suboperators,

$$\Omega_i^k = \left(\Omega_i^k\right)^{(3)}\left[\left(\Omega_i^k\right)^{(1)} + \left(\Omega_i^k\right)^{(2)}\right]. \tag{3}$$

In the aforementioned equation, $(\Omega_i^k)^{(1)}$ is the standard collisional operator, $(\Omega_i^k)^{(2)}$ is the perturbation operator contributing to the interfacial tension, and $(\Omega_i^k)^{(3)}$ is the recoloring operator promoting the segregation among the species while minimizing the lattice pinning effect.

The first suboperator, $(\Omega_i^k)^{(1)}$ describes the standard Bhatnagar-Gross-Krook collision process of the single-phase LBM where the distribution functions are relaxed towards a local equilibrium:

$$\left(\Omega_i^k\right)^{(1)}\left(f_i^k\right) = f_i^k - \left(f_i^k - f_i^{k(eq)}\right)/\tau_k. \tag{4}$$

Here, τ_k is the dimensionless relaxation time of fluid k, which is connected to the kinematic viscosity of the fluid $\nu_k = c_s^2(\tau_k - 1/2)\Delta t$. Δx and Δt are the lattice spacing and time step, respectively, and $c_s = \sqrt{1/3}\Delta x/\Delta t$ is the speed of sound for the fluid. For simplicity, $\Delta x = 1$ and $\Delta t = 1$ are used hereafter. The equilibrium distribution function $f_i^{(eq)}$ must be chosen to satisfy the conservation of mass and momentum principles. In the study, we followed the form suggested by Leclaire *et al.* [27,28,38]:

$$f_i^{k(eq)}(\rho_k, \mathbf{u}, \alpha_k) = \rho_k\left(\phi_i^k + W_i\left[\frac{\mathbf{c}_i\cdot\mathbf{u}}{c_s^2} + \frac{(\mathbf{c}_i\cdot\mathbf{u})^2}{2c_s^4} - \frac{\mathbf{u}\cdot\mathbf{u}}{2c_s^2}\right]\right). \tag{5}$$

For the D2Q9 model, the lattice weight W_i and the parameter ϕ_i^k are defined as follows:

$$W_i = \begin{cases} 4/9, & i = 0 \\ 1/9, & i = 1{-}4 \\ 1/36, & i = 5{-}8 \end{cases}, \tag{6}$$

$$\phi_i^k = \begin{cases} \alpha_k, & i = 0 \\ (1-\alpha_k)/5, & i = 1{-}4 \\ (1-\alpha_k)/20, & i = 5{-}8 \end{cases}. \tag{7}$$

The density of the fluid k is obtained from the first moment of the distribution functions

$$\rho^k = \sum_i f_i^k = \sum_i f_i^{k(eq)}, \tag{8}$$

where $f_i^{k(eq)}$ is a distribution function at the equilibrium state. The total fluid density is given by $\rho = \sum_k \rho^k$ while the total momentum is defined as the second moment of the distribution functions

$$\rho\mathbf{u} = \sum_i\sum_k f_i^k\mathbf{c}_i = \sum_i\sum_k f_i^{k(eq)}\mathbf{c}_i. \tag{9}$$

Here, $\mathbf{u}$ denotes the density weighted average velocity of the fluid.

As introduced in previous reports [27,28,38], the different density ratio γ_{kl} between fluids k and l must obey the following rule in the CGLBM to maintain a stable interface:

$$\gamma_{kl} = \frac{\rho_k^0}{\rho_l^0} = \frac{1-\alpha_l}{1-\alpha_k}, \tag{10}$$

where ρ_k^0 is the initial density of fluid k in the beginning of the simulation. In the above expressions, α is the free parameter ($0 < \alpha_k \leqslant \alpha_l < 1$ for $\rho_k^0 \leqslant \rho_l^0$).

Finally, the pressure of the fluid k is obtained by

$$p_k = \frac{3\rho_k(1-\alpha_k)}{5}. \tag{11}$$

In the CGLBM, the interfacial tension is incorporated by the perturbation operator. Here, we follow Leclaire *et al.* to model a three component system with the main equation given by

$$\left(\Omega_i^k\right)^{(2)}\left(f_i^k\right) = f_i^k + \sum_{\substack{l \\ l\neq k}} \frac{A_{kl}C_{kl}}{2}|\mathbf{F}_{kl}|\left[W_i\frac{(\mathbf{F}_{kl}\cdot\mathbf{c}_i)^2}{|\mathbf{F}_{kl}|^2} - B_i\right], \tag{12}$$

where

$$B_i = \begin{cases} -4/27, & i = 0 \\ 2/27, & i = 1{-}4 \\ 5/108, & i = 5{-}8 \end{cases}. \tag{13}$$

C_{kl} is a concentration factor that limits the activation of the surface tension at the fluid interface where both fluids k and l are present:

$$C_{kl} = \min\left\{10^6\frac{\rho_k\rho_l}{\rho_k^0\rho_l^0}, 1\right\}. \tag{14}$$

A color gradient $\mathbf{F}_{kl}$ that approximates the interface normal is defined for each fluid interface. Even though there are several forms of $\mathbf{F}_{kl}$, it has been reported that only the form below leads to physically reasonable results in a three component system [38]:

$$\mathbf{F}_{kl} = \frac{\rho_l}{\rho}\nabla\left(\frac{\rho_k}{\rho}\right) - \frac{\rho_k}{\rho}\nabla\left(\frac{\rho_l}{\rho}\right). \tag{15}$$

Here, we use an eighth-order isotropic discretization [38] to calculate the gradient of the density fraction (ρ_k/ρ) of each fluid.

Following a theoretical development by Reis and Phillips [26] with their predecessors [39], it becomes possible to predict the interfacial tension between fluids from the basic model parameters. It has been noticed that its form is also related to the gradient operator form [38]. With the gradient operator given in Eq. (15), the interfacial tension between fluids k and l is defined as

$$\sigma_{kl} = \tfrac{1}{9}(A_{kl} + A_{lk})\tau, \tag{16}$$

where $A_{kl} = A_{lk}$.

The recoloring operator is used to minimize the mixing between the fluids while keeping the laws of mass conservation and momentum. The operator is a combination of the ideas presented in Refs. [27,40] as described by

$$\left(\Omega_i^k\right)^{(3)}\left(f_i^k\right) = \frac{\rho_k}{\rho} f_i + \sum_{\substack{l \\ l \neq k}} \beta_{kl} \frac{\rho_k \rho_l}{\rho^2} \cos\left(\varphi_i^{kl}\right) f_i^{eq}(\rho, 0, \bar{\alpha}_{kl}). \tag{17}$$

Here, β_{kl} is a segregation parameter that controls the thickness of the fluids k and l interface. The variable φ_i^{kl} corresponds to the angle between the color gradient $\mathbf{F}_{kl}$ and the lattice velocity vectors $\mathbf{c}_i$. The equilibrium distribution of the fluid $f_i^{eq}(\rho, 0, \bar{\alpha}_{kl})$ can be evaluated by Eq. (5) with a zero velocity, the total density, and the density weighted average $\bar{\alpha}$. For fluids k and l, $\bar{\alpha}_{kl}$ is given by

$$\bar{\alpha}_{kl} = \frac{\rho_k}{\rho_k + \rho_l}\alpha_k + \frac{\rho_l}{\rho_k + \rho_l}\alpha_l. \tag{18}$$

Even though β_{kl} is a free parameter, it has to be carefully handled for the three component systems. At the three-phase junction, three interfacial tensions yield a Neumann's triangle, so the equilibrium contact angle θ_{kl} of fluids k and l is related to the interfacial tension by

$$\cos(\theta_{kl}) = \frac{\sigma_{mk}^2 + \sigma_{ml}^2 - \sigma_{kl}^2}{2\sigma_{mk}\sigma_{ml}}. \tag{19}$$

Spencer *et al.* [41] theoretically demonstrated that at the three-phase junction, a relation should be satisfied between θ_{kl} and the (relative) interface thickness controlled by the segregation parameter β_{kl}. Different forms of β_{kl} have been provided in the literature, and we follow the most improved form suggested by Leclaire *et al.* [38]. For fluids k and l, β_{kl} is defined as below, where β_0 is a constant between 0 and 1:

$$\beta_{kl} = \begin{cases} \beta_0, & k \text{ with } \theta_{\max} \\ \beta_0(1 + C_{\text{triple}}(\sin(\pi - \theta_{\max} - \theta_{kl}) - 1)), & \text{otherwise} \end{cases}, \tag{20}$$

where

$$C_{\text{triple}} = \min\left\{35\frac{\rho_A \rho_B \rho_C}{\rho^3}, 1\right\}. \tag{21}$$

B. Smoothed profile method (SPM)

The SPM is a promising scheme to describe particle dynamics with multibody hydrodynamic interactions [31,32]. Recently, this method has been combined with LBM and has been applied for various applications, such as rheology of concentrated suspensions [42,43], particle dynamics in viscoelastic fluids [44], and the deposition process of sticky particles in the channel flow [45].

In SPM, the boundary between solid particle and the host solvent is described by a continuous interface, which is in the form of a truncated hyperbolic function. With this numerical scheme, the discontinuity problem that arises near the boundary of the solid object can be dramatically reduced. In this work, a profile function ϕ_P is defined as below:

$$\phi_P(\mathbf{x}) = \frac{1}{2}\left[1 + \tanh\left(\frac{a - |\mathbf{x} - \mathbf{X}|}{\xi}\right)\right]. \tag{22}$$

Here, a denotes the radius of the solid particle, $\mathbf{X}$ is the center of mass of the solid particle, and $\mathbf{x}$ is the position of the lattice node. In the solvent region, $\phi_P = 0$ while $\phi_P = 1$ in the solid particle region and it continuously changes near the interfacial region. The interface thickness is determined by the parameter ξ, which we set as $\xi = \Delta x$ following previous reports [31,32,42–45].

The solvent-solid interaction force on the node $\mathbf{x}$, which is covered by a solid particle, is obtained by Eq. (23) with the assumption that the force is distributed during the time interval Δt.

$$\mathbf{f}_P(\mathbf{x}, t) = \phi_P(\mathbf{x}, t)[\mathbf{u}^*(\mathbf{x}, t) - \mathbf{u}_P(\mathbf{x}, t)]/\Delta t, \tag{23}$$

where $\mathbf{u}^*$ denotes the intermediate velocity of the solvent node calculated from the updated distribution functions obtained from the whole collision operations shown in Eq. (3). By adopting the intermediate velocity, we can include the capillary contribution into the solvent velocity at the intermediate time. This strategy is basically the same as Lecrivain *et al.*, which couples SPM with a free-energy based fluid model [46,47]. In our system, an exact form of the intermediate velocity is given by

$$\mathbf{u}^* = \frac{1}{\rho^*}\sum_i \sum_k f_i^{k,*}\mathbf{c}_i, \tag{24}$$

where $f_i^{k,*} = f_i^k + \Omega_i^k(f_i^k)$ and $\rho^* = \sum_i \sum_k f_i^{k,*}$.

$\mathbf{u}_P$ is the velocity at the solid node $\mathbf{x}$ defined in terms of the translation velocity $\mathbf{U}$ and the angular velocity $\mathbf{\Omega}$ of the solid particle as below:

$$\mathbf{u}_P(\mathbf{x}, t) = \mathbf{U} + \mathbf{\Omega} \times (\mathbf{x} - \mathbf{X}). \tag{25}$$

The hydrodynamic force at the lattice node $\mathbf{x}$ is given as

$$\mathbf{f}_H(\mathbf{x}, t) = -\mathbf{f}_P(\mathbf{x}, t). \tag{26}$$

The hydrodynamic force $\mathbf{f}_H$ is added as a body force into the LBM to consider the interactions between solid-solvent phases, which is implemented in Eq. (1) in the form of $F_i = W_i/c_s^2(\mathbf{f}_H \cdot \mathbf{c}_i)$.

Because the contribution by capillary interaction is accounted for in the calculation of intermediate velocity given in Eq. (24), the summation of hydrodynamic force and torque with capillary force is given by

$$\mathbf{F}_H + \mathbf{F}_C = \sum_{\mathbf{x} \in V_p} \rho(\mathbf{x})\mathbf{f}_P(\mathbf{x}, t), \tag{27}$$

$$\mathbf{T}_H + \mathbf{T}_C = \sum_{\mathbf{x} \in V_p} (\mathbf{x} - \mathbf{X}) \times \rho(\mathbf{x})\mathbf{f}_P(\mathbf{x}, t). \tag{28}$$

The translational velocity and angular velocity of the solid particles at a new time step are calculated by

$$\mathbf{U}(t + \Delta t) = \mathbf{U}(t) + \frac{(\mathbf{F}_H + \mathbf{F}_C)}{M_P}\Delta t, \tag{29}$$

$$\mathbf{\Omega}(t + \Delta t) = \mathbf{\Omega}(t) + \frac{(\mathbf{T}_H + \mathbf{T}_C)}{I_P}\Delta t. \tag{30}$$

Here, the mass of a solid particle and the moment of inertia are defined as $M_P = \rho_P \pi a^2$ and $I_P = 0.5 M_P a^2$, respectively, where ρ_P is the density of the solid particle.

Finally, the particle position is updated by

$$\mathbf{X}(t + \Delta t) = \mathbf{X}(t) + \mathbf{U}(t + \Delta t)\Delta t. \tag{31}$$

C. Additional coupling scheme

This section covers additional coupling algorithms not described in previous sections. The equations described in the previous sections take into account the momentum transfer between solid particles and fluids. Apart from this, an additional numerical scheme is required to keep solid particles entrapped in the fluid C phase shown in the schematic diagram (Fig. 1). In our numerical algorithm, it is implemented by the fluid C phase being fully wetted with the solid particle. To describe the wetting between the solid particle and fluid C, we follow the strategy proposed by Latva-Kokko and Rothman [25,48], which is one of the conventional methods to consider the wetting boundary condition in the CGLBM framework. In detail, it is implemented by replacing the density of the fluid to the ghost density in the calculation of the color gradient function when the wall or solid boundary nodes exist around the fluid node. In our algorithm, which considers the solid particles, the product of the smoothed profile ϕ_P and the density of the solid particle ρ_P is substituted to the ghost density in the original algorithm of Latva-Kokko and Rothman. Then, the color gradient function presented in Eq. (15) is modified as follows:

$$\mathbf{F}_{pl} = \frac{\rho_l}{\rho}\nabla\left(\frac{\rho_p\phi_P}{\rho}\right) - \frac{\rho_p\phi_P}{\rho}\nabla\left(\frac{\rho_l}{\rho}\right). \tag{32}$$

In the process, the total density also has to be recalculated from $\rho = \rho_A + \rho_B + \rho_P\phi_P$ at the lattice nodes covered by solid particles.

Simple tests were conducted to qualitatively determine how the presence or absence of particles affects. The simulation was carried out under the following conditions (all the parameters are given by the lattice unit). The simulation domain size was $L \times L$ ($L = 150$) and the no-slip boundary condition was applied at the upper and lower walls with the periodic boundary condition to the lateral direction. The fluid density (fluids A, B, and C) was set as unity ($\alpha_A = \alpha_B = \alpha_C = 4/9$) and the kinematic viscosity was $\nu = 1/6(\tau = 1)$. The same interfacial tension $\sigma_{AB} = \sigma_{BC} = \sigma_{AC} = 0.011$ was imposed and the thickness parameter $\beta_0 = 0.7$ was used. The radius of the particle was $a = 20$ and its density was the same with fluids. A detailed description of the selected parameters is provided later in Sec. III.

The density fields of fluids are plotted in Fig. 2. In the absence of particles, fluid C lies in the fluids A–B interface with the elliptical lens form at the equilibrium state [Fig. 2(a)]. On the other hand, fluid C forms the shape of a circle at the interface when the solid particle is included [Fig. 2(b)]. From this result, we confirm that our algorithm effectively transforms the shape of phase C to the solid particle while maintaining stable interfaces.

III. RESULTS AND DISCUSSION

A. Wetting test with a single particle

We carried out more systematic tests to validate our algorithm. At first, we explore the wetting of a single solid particle at the fluid interface. In the test, we focus on how the change of interfacial tension among the components affects the wetting behavior of a solid particle and also whether simulation results correctly resolve the theoretical prediction. Wetting parameters can be defined from the relative intensities of interfacial tensions among fluids and a solid particle as shown in Eq. (33). By assuming that the effect of particle weight is negligible, the contact angle θ of a particle can be calculated according to the Young-Dupré law. Furthermore, by a simple geometrical consideration like a flat fluid interface, the equilibrium position of the solid particle h^{eq} is given by

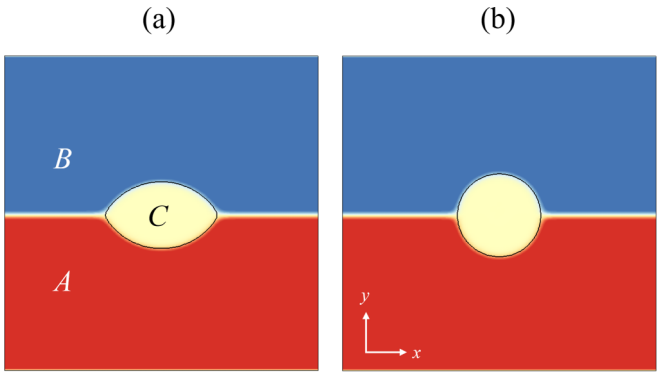

FIG. 2. Density field of fluids A, B, and C at the equilibrium state (a) without a solid particle and (b) with a solid particle (the present algorithm). The solid line (inside of fluid C) corresponds to $\rho_C = 0.5$.

$$\chi = \frac{\sigma_{BS} - \sigma_{AS}}{\sigma_{AB}} = \cos\theta = \frac{h^{eq}}{a}, \tag{33}$$

where subscripts A and B denote fluids and S (C) is the solid particle.

The size of the simulation domain was $L \times L$ ($L = 200$) and no-slip boundary condition was imposed at the upper and lower walls with a periodic boundary condition to the lateral direction. As in the previous section, the density of the fluid was unity and the same kinematic viscosity $\nu = 1/6$ was used. The particle radius was $a = 20$ and the same density was used for the solid particle. In this section, we tested the wettability of solid particles at the fluid interface implemented by the control of interfacial tensions among fluids and a solid particle. For the sake of simplicity, only σ_{BC} and σ_{AC} were controlled in the ranges σ_{AB} to $1.8\sigma_{AB}$(with an interval $0.1\sigma_{AB}$) at fixed $\sigma_{AB} = 0.011$. In addition, the thickness parameter was fixed at $\beta_0 = 0.7$. These simulation parameters correspond to a real system where a 1-μm diameter particle is floated at the fluid interface in 5 μm $\times$ 5 μm size of the domain. The density of both fluid and particle is 1000 kg/m^3 and the kinematic viscosity of the fluid is 10^{-6} m^2/s. The interfacial tension between fluids A and B corresponds to 0.032 N/m.

The density fields of fluids and a solid particle are shown in Fig. 3(a). For the wetting parameter $\chi = 0$, the solid particle maintains a neutral position at the fluid interface. With an increase in the wetting parameter, for $\sigma_{AC} < \sigma_{BC}$, the solid particle is more immersed into the fluid A phase due to the strong affinity for each other. These results show that our method can deal with the wettability of the solid particle effectively. For a more quantitative analysis, we measured

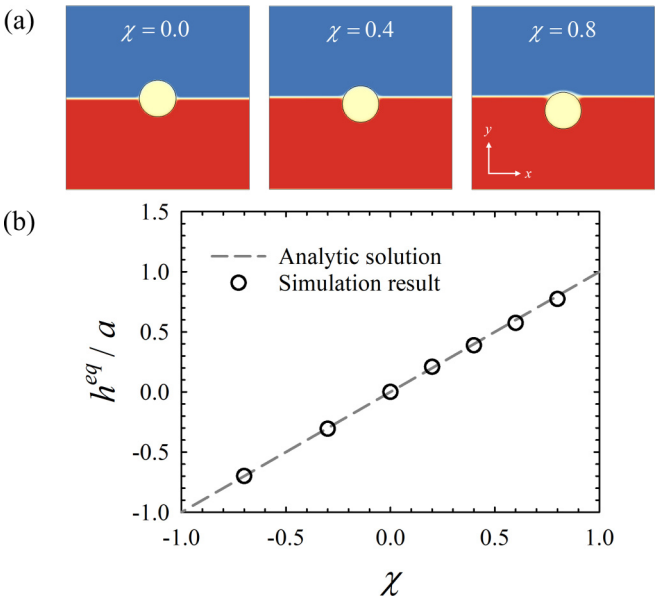

FIG. 3. The equilibrium particle position for various wetting parameters. (a) Density field of fluids with a solid particle at equilibrium. (b) (Normalized) equilibrium height of the solid particle versus the wetting parameter.

the equilibrium position of the solid particle and compared them to the analytic solution predicted by Eq. (33). As seen in Fig. 3(b), the linear correlation between the equilibrium position and wetting parameter is observed and the simulation results are almost identical to the theoretical predictions. Therefore, we confirm that the wetting of a solid particle could be well simulated with our numerical algorithm.

We also need to note the physical robustness of the wetting parameter and interfacial tension in the present method. Onishi *et al.* [8] carried out similar tests to see the effect of wetting on the solid particle. From their numerical approach, a correlation between the wetting parameter and the equilibrium height of solid particles was obtained. However, they used the mesoscopic interaction parameter "G" instead of interfacial tension in defining the wetting parameter. Thus, as mentioned by themselves, the relationship between the interaction parameter and interfacial tension is not quite obvious in their method. This implies a lack of physical robustness for that particular method and also in similar approaches [10,14] based on the SC model. In Jansen and Harting's method [14], the wettability of the solid particle is controlled by "particle color" (a virtual fluid inside of the solid particle) in addition to interaction parameter G. Although the linear relationship between particle color and wettability is captured for some limited conditions [Fig. 4(b) of Ref. [14]), basically, wettability is a combination of two variables (interaction parameter G and particle color). Because of these inherent features in the method, it is difficult to clearly figure out a physical correlation between interfacial tension and the two variables. Additionally, it limits setting a wetting condition without an antecedent parameter study. Lecrivain *et al.* [46] combined SPM with a free-energy based model (the Ginzburg-Landau type) to describe a similar system. In their method, the interfacial energy of each phase is controlled by "Cahn number" defined by relative interfacial length scales. It was shown that the wettability of the solid particles varies with Cahn numbers, but it could not achieve correct analytical predictions even by increasing the resolution of the computational grid in their test ranges.

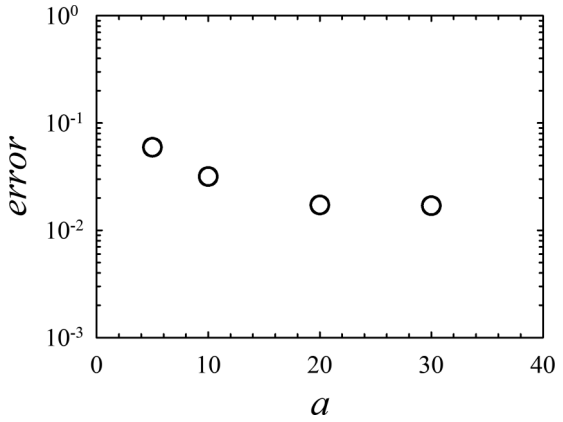

FIG. 4. L_2 norm error for the lattice grid resolution.

While there exists physical ambiguity in previous studies, the wettability on the solid particle is directly controlled by the interfacial tension in our method. Furthermore, this method shows more accurate results in the wettability prediction of the solid particle than the previous SPM-based method.

Next, we carried out an error analysis to see the convergence with the lattice grid resolution. In the test, the simulation domain size was $L = 10a$ and particle radii of $a = 5$, 10, 20, and 30 were considered. As the particle radius increases from $a = 5$ to 30, the total number of lattice grids in the simulation domain increases from 50×50 to 300×300, which means that an increase of particle size corresponds to a higher grid resolution in the test system. The same parameters were used as in the previous test, except for domain size and particle radius. For the quantification of results, we introduce L_2 norm error for each grid resolution, which is calculated from the equation below:

$$\text{error}(A) = \sqrt{\frac{1}{N}\sum_{i=1}^{N} |A_{i,\text{LBM}} - A_{i,\text{Analytical}}|^2}\,. \tag{34}$$

Here, A_{LBM} and $A_{\text{Analytical}}$ denote h^{eq}/a obtained by LBM simulation and the analytical solution by Eq. (33), respectively. Error analysis was performed for 9 data points ($N = 9$) in the range $-0.8 \leqslant \chi \leqslant 0.8$ (with 0.2 intervals).

The result is plotted in Fig. 4. The lowest grid resolution, $a = 5$ shows an error of about 5.93% and the accuracy of the solution is improved by increasing grid resolution. When $a = 20$, the error is about 1.72%, which is not much different from the error value 1.69% at a higher resolution $a = 30$. We obtained convergence for a large than 20 and maintained this grid resolution for most of the tests covered in the following parts.

In the CGLBM, the solution accuracy is known to change according to the parameter β_0, which determines the thickness of the fluid interface. For the two-phase system (without solid particle), $\beta_0 = 0.7$ has been suggested as an optimum value to obtain the most accurate and stable solutions [18,28,29,38].

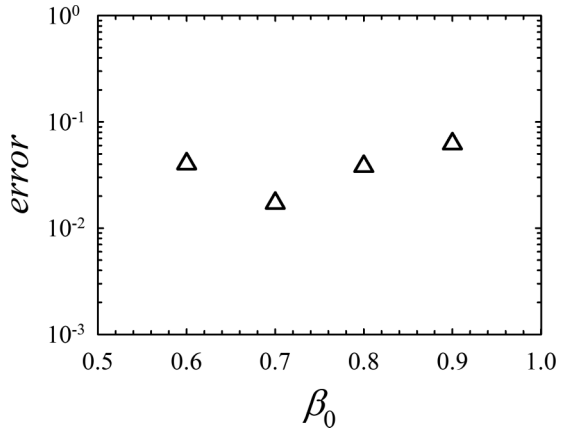

FIG. 5. L_2 norm error as a function of parameter β_0.

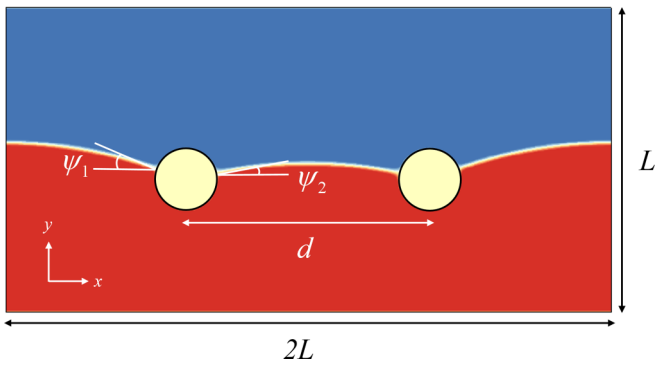

FIG. 6. Schematic diagram of the simulation system: two heavy particles floating at the fluid interface with interparticle distance d. ψ_1 and ψ_2 denote contact angles around the solid particle.

We assume that the error dependence for the parameter β_0 may also exist in the present model where solid particles and fluids are coupled. Therefore, we carried out further tests to confirm this where the simulation condition was the same as the first one in this section ($L = 200$ and $a = 20$), but only the parameter β_0 was changed for ranges $\beta_0 = 0.6-0.9$ (with 0.1 intervals).

The result is shown in Fig. 5. The smallest error is obtained at $\beta_0 = 0.7$ as in previous reports regarding two component systems [18,28,29,38]. Based on the present results, we confirm that $\beta_0 = 0.7$ is still optimal even in our method, so we decided to use this parameter value for all the tests that follow. Although the physical meaning and correlation between observed errors and parameter β_0 have not been fully discussed in this test, it should be addressed in future studies.

B. Capillary interactions between two particles

As a next step, we carried out the simulation test to see whether the capillary interactions between the particles is correctly resolved in our algorithm. In previous tests, the particles' weight was ignored and the fluid interface remained flat at equilibrium. When the weight of the particle cannot be neglected, for example, due to unequal density between the particles and fluids, it could induce deformation of the fluid interface. The interface deformation would give rise to the capillary interactions among the particles residing at the same interface [8,49,50]. In this section, we investigate capillary interactions between two solid particles floating at the fluid interface. We consider the system as illustrated in Fig. 6 and carefully analyze the change of contact angle and particle motion induced by the capillary interactions for different interparticle distances.

First, we consider the case with interparticle distance $d = L$. When the initial interparticle separation is half of the simulation domain such that $d = L$ (see Fig. 6), all the lateral motion (for x direction in our system) of the solid particle is prohibited by the symmetry of the capillary interactions due to the periodicity of the simulation domain [8]. In this case, the contact angle has the same value $\psi^{eq}(=\psi_1^{eq} = \psi_2^{eq})$ on both sides of the particle due to the symmetry of capillary interaction. The only vertical motion in particles is allowed and their position is determined by the balance between the buoyancy force and the interfacial tension. The correlation between equilibrium contact angle ψ^{eq} and gravitational acceleration g is given by

$$2\sigma_{AB} \sin \psi^{eq} = \pi a^2 g(\rho_p - \rho_f), \tag{35}$$

where ρ_p and ρ_f are the densities of solid particle and fluid, respectively.

The relative intensity of gravitational acceleration and interfacial tension can be described by the Bond number (Bo).

$$\mathrm{Bo} = \frac{(\rho_p - \rho_f)ga^2}{\sigma_{AB}}. \tag{36}$$

Finally, from Eqs. (35) and (36), the equilibrium contact angle can be described as a function of Bond number as below:

$$\psi^{eq} = \sin^{-1}\left(\frac{\pi}{2}\mathrm{Bo}\right). \tag{37}$$

The simulation conditions are as follows. The simulation domain size was $2L \times L$ ($L = 200$) with the same boundary condition as before. The kinematic viscosity was $\nu = 1/6$ and the interfacial tension was $\sigma_{AB} = \sigma_{BC} = \sigma_{AC} = 0.011$ (the neutral wetting condition for the solid particles). In the test, we considered two heavy solid particles to observe the effect of gravity on the particles floating at the fluid interface (Fig. 6). The density of the solid particle was set to two times larger than fluids A and B ($\rho_P = 2$). The density of fluid C must be matched to the particle density such that $\rho_P = \rho_C$. To satisfy the rule in Eq. (10), free parameters were set as $\alpha_A = \alpha_B = 1/3$ and $\alpha_C = 2/3$. The particle radius was $a = 20$ and the interface thickness parameter $\beta_0 = 0.7$ was used as in previous tests.

At the beginning of the simulation, two solid particles float at the fluid interface (in the midst of the simulation domain) without any acceleration until it reaches the equilibrium state. Then, the gravitational acceleration was applied to two solid particles in the range of $\mathrm{Bo} = 0.01-0.4$. The density fields are shown in Fig. 7(a) for the representative cases ($\mathrm{Bo} = 0.1$ and 0.4). At $\mathrm{Bo} = 0.4$, a significant change in the particles' equilibrium position and the curvature of the fluid interface is observed while a tiny change at $\mathrm{Bo} = 0.1$. With the increased Bond number, a larger contact angle is observed, but the

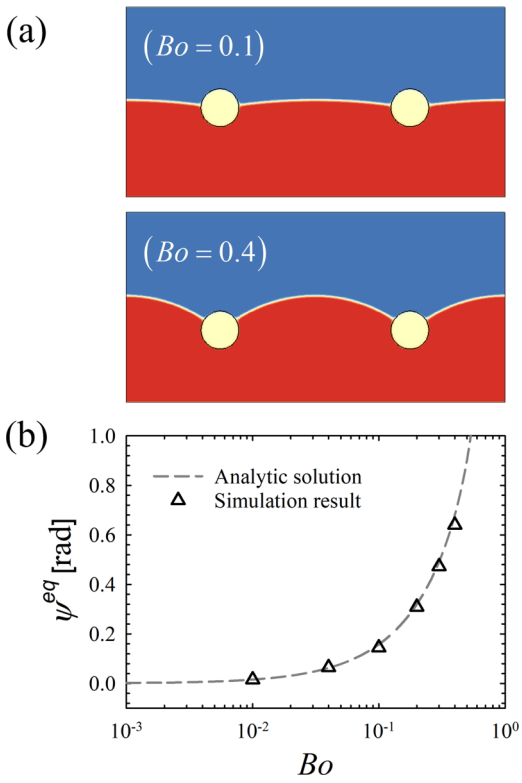

FIG. 7. (a) Simulation results for Bo = 0.1 and 0.4. (b) The equilibrium contact angle of the particle (ψ^{eq}) versus the Bond number (Bo). The triangle is the simulation result and the grey dashed line is an analytic solution predicted by Eq. (37).

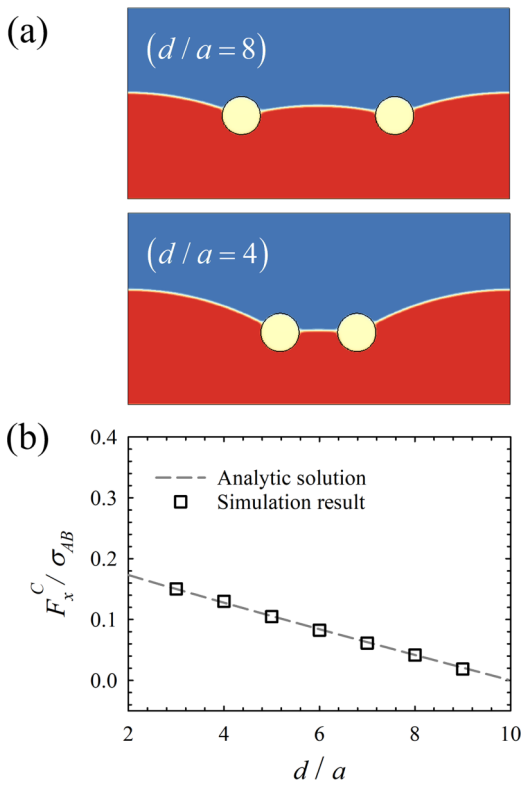

FIG. 8. (a) Simulation results for interparticle distances $d/a = 8$ and $d/a = 4$ (Bo = 0.2). (b) Capillary interactions for the lateral directions versus interparticle distance (both dimensionless forms). The square symbol is the simulation result and the grey dashed line is the analytic solution obtained by Eqs. (38)–(41).

values on both sides of the solid particles are still the same. These results demonstrate that the symmetry of the capillary interactions correctly work in the periodic domain and also imply that the gravitational acceleration qualitatively works in our numerical method. For the quantitative analysis, we investigated the correlation between contact angle and Bond number. The contact angle was obtained from the tangential slope of the fluid interface. As shown in Fig. 7(b), the contact angle exponentially increases with Bond numbers in the test ranges. Our simulation results correspond well to the analytic solution predicted by Eq. (37).

Next, we explored the capillary interactions in terms of the interparticle distance. By changing the interparticle distance, the symmetry of the capillary force is no longer maintained and the particles have two different equilibrium contact angles ψ_1^{eq} and ψ_2^{eq}. In this case, Eq. (37) can be rewritten as

$$\sin\left(\psi_1^{eq}\right) + \sin\left(\psi_2^{eq}\right) = \pi \mathrm{Bo}. \tag{38}$$

To obtain the contact angle, both hydrostatic equilibrium conditions for the fluid interface and the geometrical restriction for the particles must be considered. From the rule of the hydrostatic conditions, the interface curvature at positions P_1 and P_2 should be equal and the interface curvature is $R_1 = R_2 = R_{\mathrm{int}}$. R_{int} can be obtained by substituting Eqs. (39) and (40) into Eq. (38), then each of the contact angles can be obtained at the specific Bond number and interparticle distance:

$$\sin\left(\psi_1^{eq}\right) = \frac{d}{2R_{\mathrm{int}}}, \tag{39}$$

$$\sin\left(\psi_2^{eq}\right) = \frac{2L - d}{2R_{\mathrm{int}}}. \tag{40}$$

Finally, the capillary force (lateral force) acting on the particles can be evaluated as a function of contact angle and interfacial tension between fluids A and B as below [8]:

$$F_x^C = \sigma_{AB}\left[\cos\left(\psi_1^{eq}\right) - \cos\left(\psi_2^{eq}\right)\right]. \tag{41}$$

We carried out the test to quantitatively validate the capillary interactions within our simulation algorithm. The interparticle distance in the range of $d = 3a - 9a$ was considered and other conditions were set as in the previous test. By changing the interparticle distance, the symmetry of the capillary force is broken, which leads to difficulties in measuring the capillary force at the specific interparticle distance. To solve this issue, the lateral motion of the particle was constrained in the test. Therefore, the particles are allowed to move only in the vertical direction following the strategy of Onishi *et al.* [8]. After the system reaches the equilibrium state, (gravitational) acceleration corresponding to Bo = 0.2 was applied to two solid particles.

As seen in Fig. 8(a), changes in the curvature of fluid interface and contact angle are observed. In particular, at the

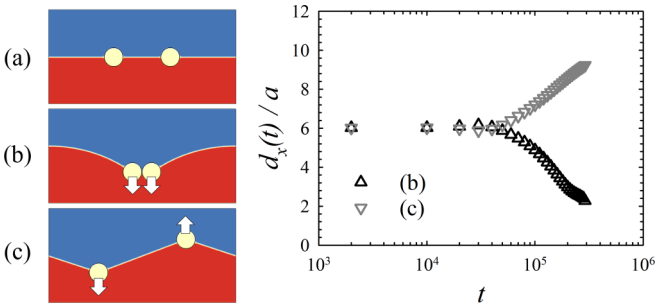

FIG. 9. The lateral particle motion induced by capillary interaction. (a) Initial particle configuration. (b) The particles are vertically accelerated in the same direction. (c) The particles are accelerated vertically in the opposite direction. The right side of the figure describes temporal particle separation in the lateral direction.

small interparticle gap $d/a = 4$, a strong distortion in the fluid interface is captured with quite a difference in contact angles for both sides of solid particles. We evaluated the equilibrium contact angle in the same way with the previous test and plotted it as a form of the capillary force provided in Eq. (41). As shown in Fig. 8(b), the capillary force increases with a decrease in interparticle distance, and the simulation result shows a good agreement with the predictions in Eqs. (38)−(41).

As far as we are concerned, any quantitative analysis for capillary interactions between two particles has never been performed in several LBM [10,14] or SPM based methods [46,47]. This implies that there has been ambiguity in the prediction of the capillary interactions among solid particles in previous studies. On the other hand, our method is validated well in that respect, which supports the theoretical and numerical robustness of the present method.

We additionally tested the capillary lateral motion of two solid particles at the fluid interface. The simulation domain, boundary condition, and the material properties are the same as in the previous test, but the particle motion for the lateral direction was not constrained anymore. To prevent overlap between particles, we applied the Weeks-Chandler-Andersen (WCA) type of potential [51] with a lubrication correction term [52,53]. In this test, we consider two sets of the situation: one where both particles are accelerated vertically in the same direction (toward the bottom wall) and the other where the particles are accelerated vertically in the opposite direction. Simulation results are provided in Fig. 9. For the former case, two particles attract each other [Fig. 9(b)], while in the latter they push against [Fig. 9(c)]. These phenomena follow the prediction of the capillary charge theory between two particles and also qualitatively match with experimental observations [8,49,50,54]. We also analyzed the temporal motion of the particles in the lateral direction (right side of Fig. 9). At the early stage ($t \leqslant 10^4$), the particles hardly move at the interface and then start to move in opposite directions ($t \sim 2 \times 10^4$). In the next stage, sudden acceleration (exponential) is observed in both systems ($3 \times 10^4 < t \leqslant 2 \times 10^5$), and finally, they reach the steady state. As seen in the results, even for the two particles system, the dynamics caused by capillary interactions is quite complicated.

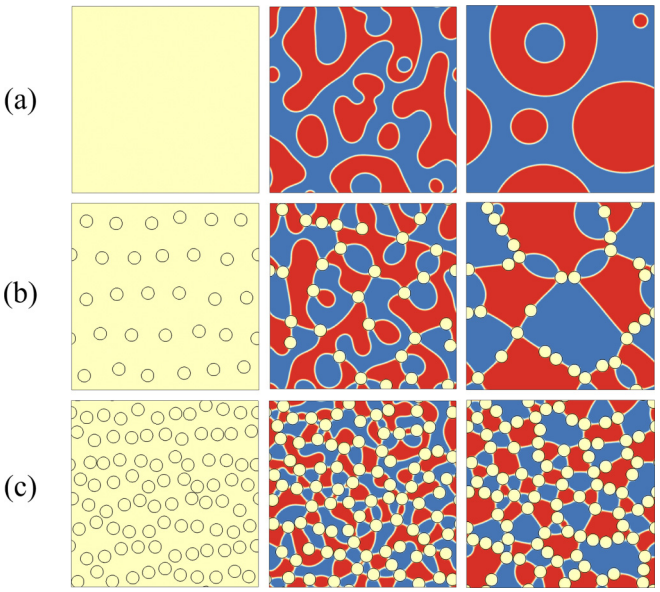

FIG. 10. Spinodal decomposition of fluid mixtures. (a) Binary ($\phi = 0$), (b) ternary ($\phi = 0.1$), and (c) ternary ($\phi = 0.3$) mixtures. Results correspond to $t = 0$, $t = 50000$, and $t = 600000$ from left to right.

C. Application: Spinodal decomposition of the ternary mixture

In previous sections, we performed several simulation tests including the wetting of a single solid particle and the capillary interactions in two solid particles floating at the fluid interface. From these analyses, we confirmed that the key features of the particle dynamics at the fluid interface are correctly resolved in our simulation method.

We now apply the presented method to a further complicated situation: spinodal decomposition of a ternary mixture. Spinodal decomposition can be viewed as a physical process of phase separation of emulsions. Also, this is one of the good benchmark problems that can test the stability and robustness of the multiphase models [55–57]. We set the system for the spinodal decomposition of a ternary mixture, in particular, which contains two-immiscible fluids with solid particles. Through this test, we try to look into the parts that were not covered in previous tests and to see the potential of the algorithm toward soft matter systems from a qualitative point of view.

The simulation condition are given as follows. The domain size was $L \times L$ ($L = 300$) and periodic boundary conditions were applied for both the x and y directions. The kinematic viscosity was $\nu = 1/6$ and the interfacial tension was set to $\sigma_{AB} = 0.0011$. The density of the fluid was unity and free parameters were set as $\alpha_A = \alpha_B = \alpha_C = 4/9$ and $\beta_0 = 0.7$. The particle radius was $a = 10$ and the neutral wetting condition was applied ($\sigma_{BC} = \sigma_{AC}$). To prevent overlap between the particles, the WCA type of potential was applied with a lubrication correction term as in previous tests. The particle volume (area) fraction was $\phi \sim 0.1$ and 0.3. We also considered a binary liquid mixture (pure fluid mixture without solid particles) and its condition was equal to the ternary fluid mixture, except for the existence of solid particles.

The simulation results are provided in Fig. 10. In the beginning of the simulation, both fluids (the ratio of A and

B is 1:1) and solid particles are randomly distributed in the simulation domain, and the segregation starts. In a binary fluid mixture (without solid particles), relatively fast segregation is observed and a bicontinuous structure evolves during phase transition [Fig. 10(a)]. These characteristics represent the typical features of spinodal decomposition of binary fluid mixtures [23,55,56]. On the other hand, quite different behavior is captured in ternary fluid mixtures. The segregation of fluids is suppressed and more discrete structures are formed by adding solid particles in immiscible fluids [Figs. 10(b) and 10(c)]. Most solid particles are relocated to the fluid interface due to their neutral affinity with fluids and they sometimes form the "jamming" structure with trapping other fluids inside. These characteristics become clear when particle volume fractions increase.

Recently, there have been many reports on the effect of solid particles in the emulsion systems [58–62]. Solid particles stabilize the fluid interface and also affect the structure of the fluids. Depending on the proportion and affinity of the components, various morphologies such as bijels and Pickering emulsions are formed, and finally it induces dramatic changes in rheology (not presented here). These features are reflected well even in our simulation results. In particular, the captured morphology through our simulation looks quite similar to bijels (bicontinuous interfacially jammed emulsion gels) [14,58,59,61]. One of the relevant simulation results may be provided in Jansen and Harting's report [14], where they studied phase transition of fluid-solid mixtures based on the SC based LBM. They captured bijel structure at almost the same conditions of this work (the fluid ratio 1:1 and neutral wetted particles). In their results, most particles were located at the fluid interface (for neutral wetting condition) and fluids were entrapped by a jammed structure formed by solid particles (Figs. 7 and 8 of Ref. [14]). The segregation of fluids was suppressed and much smaller average domain sizes (for fluids) were captured with increasing particle volume fractions (Fig. 10 in Ref. [14]). All the mentioned features are quite similar to the results from our simulation (Fig. 10) and also correspond to other simulation and experimental results [58,59,61,63] in a qualitative sense. Although our test was carried out for limited conditions, the results captured most physics governing the phase separation of the ternary mixtures; for example, the stabilizing effect by solid particles and significant changes in morphology. From these observations, we confirm the feasibility of our numerical method to describe soft matter systems, in particular, emulsions including solid particles. Further studies will be necessary for unsolved issues, which is beyond the scope of this work.

IV. CONCLUSION

We suggest a numerical method that describes the dynamics of solid particles at fluid interfaces. The presented method was established on the CGLBM and combined with the SPM. In the proposed method, immiscible fluids were described by CGLBM and the momentum transfer among the solid particle and fluid was achieved by SPM. Although CGLBM is one of the promising methods in dealing with multiphase systems, it has never been adaptable for liquid systems involving solid particles. To combine these two existing methods, we designed a different coupling algorithm. We considered two immiscible fluids *A* and *B* along with fluid *C*, which is additionally considered to control the wettability of the solid particle at the interface. In the method, the solid particle is always entrapped in the fluid *C* phase, which was achieved by applying the fully wetted condition of fluid *C* to the solid particle.

To validate the present method (CGLBM-SPM), we performed several simulation tests. At first, the equilibrium contact angle of a single solid particle at the fluid interface was studied. The wettability of the particle was controlled by the change in interfacial tension among the components and then the change in equilibrium position of the solid particle was investigated. We defined affinity parameter (χ) from the relative interfacial tension of the components and the dependency for this parameter was carefully investigated. By controlling the affinity parameter, the equilibrium height of the solid particle was found to change, which corresponded well with the analytical solution. We also analyzed the system by using the L_2 norm error for the lattice grid resolution and interface thickness parameter. From the tests, we suggested optimized values for the lattice grid resolution ($a = 20$) and the interface thickness parameter ($\beta_0 = 0.7$). Then, we tested a more complicated system where two high-density particles are floated at the fluid interface. In that system, the contact angle of the particle and the interface curvature are determined by the balance between the buoyancy force and the interfacial tension of the fluids in addition to the interdistance between solid particles. Our simulation results reflected the previously mentioned characteristics well and also showed good agreement with the analytic solutions. The lateral motion of two solid particles induced by the capillary interactions was demonstrated as well. Depending on the accelerated direction of solid particles, both attractive and repulsive motions were captured that qualitatively followed the prediction by the capillary charge theory and experimental observation. From the simulation results, we confirmed that the capillary interactions (in the lateral direction) is correctly resolved in our numerical method. As a final example, we applied the present method to spinodal decomposition of a ternary mixture, which contains two-immiscible fluids with solid particles. By adding solid particles, the fluid segregation was much suppressed compared to the binary liquid mixture and completely different morphology was obtained like with the jamming structure of the particles at the fluid interface. Captured behaviors looked quite reasonable and similar to literature, such as "bijels" in particular. Although the test was implemented for limited cases only, the results captured most physics governing the phase separation of the ternary mixtures. Therefore, we confirmed the feasibility of the present method to describe soft matters; in particular, emulsion systems that contain solid particles at interfaces. Finally, we conclude that the dynamics of solid particles at the fluid interface can be correctly resolved by the proposed method.

ACKNOWLEDGMENTS

This work was supported by the National Research Foundation of Korea (NRF) grant funded by the Korea government (MSIT) (No. NRF-2018R1A5A1024127).

[1] K. Zahn and G. Maret, Phys. Rev. Lett. **85**, 3656 (2000).
[2] A. Bausch, M. J. Bowick, A. Cacciuto, A. Dinsmore, M. Hsu, D. Nelson, M. Nikolaides, A. Travesset, and D. Weitz, Science **299**, 1716 (2003).
[3] J. H. Fendler, Curr. Opin. Colloid Interface Sci. **1**, 202 (1996).
[4] R. Aveyard and J. H. Clint, J. Chem. Soc. Faraday Trans. **91**, 2681 (1995).
[5] B. P. Binks, Curr. Opin. Colloid Interface Sci. **7**, 21 (2002).
[6] H.-J. Butt, Science **331**, 868 (2011).
[7] E. Koos, Curr. Opin. Colloid Interface Sci. **19**, 575 (2014).
[8] J. Onishi, A. Kawasaki, Y. Chen, and H. Ohashi, Comput. Math. Appl. **55**, 1541 (2008).
[9] X. Shan and H. Chen, Phys. Rev. E **47**, 1815 (1993).
[10] A. S. Joshi and Y. Sun, Phys. Rev. E **79**, 066703 (2009).
[11] A. J. Ladd, J. Fluid Mech. **271**, 285 (1994).
[12] A. J. Ladd, J. Fluid Mech. **271**, 311 (1994).
[13] A. S. Joshi and Y. Sun, Phys. Rev. E **82**, 041401 (2010).
[14] F. Jansen and J. Harting, Phys. Rev. E **83**, 046707 (2011).
[15] G. B. Davies, T. Krüger, P. V. Coveney, J. Harting, and F. Bresme, Adv. Mater. **26**, 6715 (2014).
[16] L. Chen, Q. Kang, Y. Mu, Y.-L. He, and W.-Q. Tao, Int. J. Heat Mass Transfer **76**, 210 (2014).
[17] Q. Li, K. H. Luo, Q. J. Kang, Y. L. He, Q. Chen, and Q. Liu, Prog. Energy Combust. Sci. **52**, 62 (2016).
[18] S. Leclaire, A. Parmigiani, O. Malaspinas, B. Chopard, and J. Latt, Phys. Rev. E **95**, 033306 (2017).
[19] Y. Yu, H. Liu, D. Liang, and Y. Zhang, Phys. Fluids **31**, 012108 (2019).
[20] M. R. Swift, E. Orlandini, W. R. Osborn, and J. M. Yeomans, Phys. Rev. E **54**, 5041 (1996).
[21] X. He, X. Shan, and G. D. Doolen, Phys. Rev. E **57**, R13 (1998).
[22] A. K. Gunstensen, D. H. Rothman, S. Zaleski, and G. Zanetti, Phys. Rev. A **43**, 4320 (1991).
[23] D. H. Rothman and J. M. Keller, J. Stat. Phys. **52**, 1119 (1988).
[24] D. Grunau, S. Chen, and K. Eggert, Phys. Fluids A **5**, 2557 (1993).
[25] M. Latva-Kokko and D. H. Rothman, Phys. Rev. E **72**, 046701 (2005).
[26] T. Reis and T. N. Phillips, J. Phys. A **40**, 4033 (2007).
[27] S. Leclaire, M. Reggio, and J.-Y. Trépanier, Appl. Math. Modell. **36**, 2237 (2012).
[28] S. Leclaire, M. Reggio, and J.-Y. Trépanier, Comput. Fluids **48**, 98 (2011).
[29] H. Liu, A. J. Valocchi, and Q. Kang, Phys. Rev. E **85**, 046309 (2012).
[30] Z. X. Wen, Q. Li, Y. Yu, and K. H. Luo, Phys. Rev. E **100**, 023301 (2019).
[31] Y. Nakayama and R. Yamamoto, Phys. Rev. E **71**, 036707 (2005).
[32] K. Kim, Y. Nakayama, and R. Yamamoto, Phys. Rev. Lett. **96**, 208302 (2006).
[33] H. Liu, Q. Kang, C. R. Leonardi, S. Schmieschek, A. Narváez, B. D. Jones, J. R. Williams, A. J. Valocchi, and J. Harting, Computat. Geosci. **20**, 777 (2016).
[34] A. Montessori, M. Lauricella, E. Stolovicki, D. A. Weitz, and S. Succi, Phys. Fluids **31**, 021703 (2019).
[35] A. Montessori, M. Lauricella, A. Tiribocchi, and S. Succi, Phys. Rev. Fluids **4**, 072201 (2019).
[36] Y.-H. Fu, L. Bai, K.-H. Luo, Y. Jin, and Y. Cheng, Phys. Rev. E **95**, 043304 (2017).
[37] H. Liu, Y. Ba, L. Wu, Z. Li, G. Xi, and Y. Zhang, J. Fluid Mech. **837**, 381 (2018).
[38] S. Leclaire, M. Reggio, and J.-Y. Trépanier, J. Comput. Phys. **246**, 318 (2013).
[39] I. Halliday, S. P. Thompson, and C. M. Care, Phys. Rev. E **57**, 514 (1998).
[40] M. Latva-Kokko and D. H. Rothman, Phys. Rev. E **71**, 056702 (2005).
[41] T. J. Spencer, I. Halliday, and C. M. Care, Phys. Rev. E **82**, 066701 (2010).
[42] Y. K. Lee, K. H. Ahn, and S. J. Lee, Phys. Rev. E **90**, 062317 (2014).
[43] Y. K. Lee, J. Nam, K. Hyun, K. H. Ahn, and S. J. Lee, Soft Matter **11**, 4061 (2015).
[44] Y. K. Lee and K. H. Ahn, J. Non-Newton. Fluid **244**, 75 (2017).
[45] Y. K. Lee, C. Porter, S. L. Diamond, J. C. Crocker, and T. Sinno, J. Colloid Interface Sci. **530**, 383 (2018).
[46] G. Lecrivain, R. Yamamoto, U. Hampel, and T. Taniguchi, Phys. Fluids **28**, 083301 (2016).
[47] G. Lecrivain, R. Yamamoto, U. Hampel, and T. Taniguchi, Phys. Rev. E **95**, 063107 (2017).
[48] M. Latva-Kokko and D. H. Rothman, Phys. Rev. Lett. **98**, 254503 (2007).
[49] P. A. Kralchevsky and K. Nagayama, Langmuir **10**, 23 (1994).
[50] P. A. Kralchevsky and K. Nagayama, Adv. Colloid Interface Sci. **85**, 145 (2000).
[51] H. C. Andersen, D. Chandler, and J. D. Weeks, Adv. Chem. Phys **34**, 105 (1976).
[52] N.-Q. Nguyen and A. J. C. Ladd, Phys. Rev. E **66**, 046708 (2002).
[53] J. Kromkamp, D. van den Ende, D. Kandhai, R. van der Sman, and R. Boom, Chem. Eng. Sci. **61**, 858 (2006).
[54] P. C. Millett and Y. U. Wang, J. Colloid Interface Sci. **353**, 46 (2011).
[55] F. J. Alexander, S. Chen, and D. W. Grunau, Phys. Rev. B **48**, 634 (1993).
[56] E. Orlandini, G. Gonnella, and J. Yeomans, Physica A **240**, 277 (1997).
[57] V. M. Kendon, M. E. Cates, I. Pagonabarraga, J.-C. Desplat, and P. Bladon, J. Fluid Mech. **440**, 147 (2001).
[58] K. Stratford, R. Adhikari, I. Pagonabarraga, J.-C. Desplat, and M. E. Cates, Science **309**, 2198 (2005).
[59] E. M. Herzig, K. A. White, A. B. Schofield, W. C. K. Poon, and P. S. Clegg, Nat. Mater. **6**, 966 (2007).
[60] E. Koos and N. Willenbacher, Science **331**, 897 (2011).
[61] M. N. Lee, J. H. Thijssen, J. A. Witt, P. S. Clegg, and A. Mohraz, Adv. Funct. Mater. **23**, 417 (2013).
[62] A. Mohraz, Curr. Opin. Colloid Interface Sci. **25**, 89 (2016).
[63] J. M. Carmack and P. C. Millett, J. Chem. Phys. **143**, 154701 (2015).